

# Glass Molded Optical Interposers for Wafer Scale Datacom Component Packaging

F. Merget<sup>(1,2)</sup>, M. Ackermann<sup>(1)</sup>, B. Shen<sup>(1)</sup>, G. D. Saunders<sup>(4)</sup>, S. Haag<sup>(4)</sup>, M. Wolz<sup>(3)</sup>, J. Witzens<sup>(1,2)</sup>

<sup>(1)</sup> Chair of Integrated Photonics, RWTH Aachen, 52074 Aachen, [jwitzens@iph.rwth-aachen.de](mailto:jwitzens@iph.rwth-aachen.de)

<sup>(2)</sup> aiXscale Photonics UG, Virchowstr. 14, 50935 Köln, Germany

<sup>(3)</sup> GD Optical Competence GmbH, Herborner Strasse 7-9, 35764 Sinn, Germany

<sup>(4)</sup> Aixemtec GmbH, Kaiserstrasse 100, 52134 Herzogenrath, Germany

**Abstract** We report on glass-molded micro-optical interposers for single mode fiber-to-PIC coupling fabricated at the wafer scale that result in less than 1 dB excess insertion losses. They allow a narrow package footprint and can be extended to support polarization management, isolation and wavelength multiplexing.

## Introduction

Backend packaging and optical subassembly make up for 30% to 90% of the total manufacturing cost of optical transceivers and have been identified as the main limitation to a more rapid deployment of otherwise very scalable silicon photonics (SiP) technology<sup>[1]</sup>. This calls for an equally scalable and low cost packaging technology utilizing building blocks that can also be manufactured at the wafer scale. Moreover, growing fiber counts in parallel optics solutions also have to be supported by emerging packaging solutions. For example, MPO connectors with up to 32 fibers have now been standardized. Both the QSFP-DD800 and 800G Pluggable Multi Source Agreements (MSA) envision up to 16 fibers for 800G modules. Requirements for a growing density of fibers are further exacerbated by the emergence of co-packaged optics (CPO), in which a large number of fibers have to be crammed in a small area around the switch chip<sup>[2]</sup>. As serial data rates have been rising, the aperture of vertical cavity surface emitting lasers (VCSELs) and large area detectors (LADs) have also been shrinking to support required modulation bandwidths<sup>[3]</sup>, so that alignment tolerances are also tightening for multi-mode optics. As a result, the tolerances of plastic molded piece parts commonly used there are running into their technological limits, creating a need for glass based micro-optics manufactured at a low enough cost.

In our previous work, we have developed

alignment tolerant couplers for SiP photonic integrated circuits (PICs) applied to parallel optics transceivers<sup>[4]</sup> or external cavity lasers<sup>[5]</sup>. Here, we report on glass interposers serving to fiber couple such PICs as well as VCSELs and LADs, that can be molded, surface treated and assembled at the wafer-scale, providing a low-cost and scalable solution for the packaging of datacom modules and CPO for top-of-the-rack (TOR) switches. In addition to providing compact light routing and fiber coupling, they have been conceived to support polarization management, optical isolation and wavelength division multiplexing (WDM).

## Basic building blocks

Figure 1 shows the glass interposer concept. As represented in the schematic in panel (a), two identical glass pieces with 4 lenses each are attached to each other with UV curable index-matched epoxy. They each comprise a surface to which further elements such as a fiber array (FA), a PIC, or a VCSEL / LAD on submount can be attached, as depicted in panels (c) and (d). The lenses are recessed, so that the emitting surface of the attached element is close to their focal plane. Consequently, the light, with beam path represented by the red arrows in (a), is close to collimated inside the glass pieces and is refocused upon exiting them. A flat molded surface on one of the glass building blocks also acts as a mirror that bends the light across a 90-degree angle. Panel (b) shows a photograph

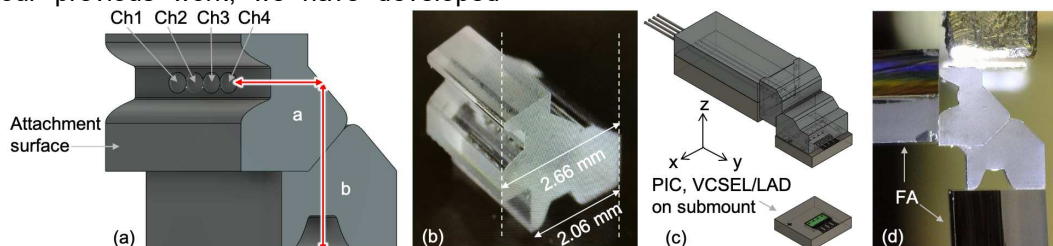


**Fig. 1:** Glass interposer concept in its simplest configuration. (a) Schematic of the glass interposer formed by attaching two glass molded building blocks. (b) Photograph of an assembled interposer. (c) Coupling of a PIC or VCSEL / LAD array on submount to an FA. (d) Single mode FA-to-FA coupling used for characterizing the interposers. The footprint of the interposer in (c) is 2.06 by 2.5 mm on the submount, its height is 2.66 mm.

of an assembled interposer and panel (d) the measurement setup used for its characterization, in which two FAs with four standard single mode fibers each (SMF-28) are coupled to each other.

The glass pieces required for these interposers are fabricated in parallel at the (glass-)wafer scale with isothermal precision glass molding<sup>[6]</sup>. Fig. 2(a) shows 100 arrays of groups of 4 lenses fabricated in a single molding step. GD-optics has developed a customized, low-cost and compact isothermal press that goes through a complete cycle in less than 20 minutes, that has since been extended to the parallel molding of over 100 arrays of 8 lenses each. With non-stop operation, over a million such interposers can be fabricated per year with a single press and the process can be straightforwardly parallelized. The density of lenses on the glass wafer can be further increased and efforts are under way to increase the wafer size. Thin film coatings as required for polarization management or WDM in the advanced interposer configurations discussed in the next section can be selectively applied at the wafer scale with shadow masking. Complex interposers can also be built up on a common glass wafer prior to singulation. As seen in Fig. 2(c), the lenses, with a 250  $\mu\text{m}$  pitch matching standard FAs, are of high quality.

As a consequence of the top and bottom surfaces of the glass pieces being formed by opposite molds, the overlay accuracy of the top and bottom surfaces as well as their spacing result in the largest tolerances in the manufacturing process, in the order of 5  $\mu\text{m}$ . Even though this is relatively large compared to the mode field diameter of SMFs or the aperture size of high-speed VCSELs and LADs, it is actually not a problem here. Coupling efficiencies are insensitive to the distance between top and bottom surfaces, since rays are routed on a cartesian grid restricted to the horizontal and vertical directions relative to the attachment surfaces / reference planes of the press. A displacement of the top surface in the vertical (z)-direction thus does not impact where and under which angle the ray is routed to in the final assembly. An overlay error in the in-plane x- and y-directions does impact ILs. However, at the top

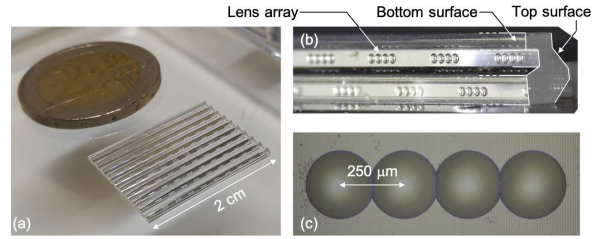


**Fig. 2:** Waferscale fabrication. (a) Photograph of a molded glass wafer. (b) Detailed photograph of a singulated row of glass building blocks. Only the top row of lenses is real, the bottom row is a mirror image created by the reflective upper surface of the micro-optical element. “Top” and “bottom” surfaces are labeled according to the main text and refer to the initial bottom and top surfaces of the unmolded glass piece, relative to the axis of the press. Here, the glass piece is photographed lying on its side. (c) Detailed microscope image of a four-lens array.

surface, defined here as the surface with the large reflective / transmissive facets as labeled in Fig. 2(b), the collimated beams have an expanded field diameter in the order of 100  $\mu\text{m}$ , so that displacements in the  $\mu\text{m}$  range do not significantly impact performance. On the other hand, the relative angular orientation of the top and bottom surfaces, that is critical for ILs, is very well controlled. A complete set of Monte-Carlo simulations has been performed with ray tracing in order to verify the viability of the technology. Since beams are collimated and expanded when crossing or being reflected by the top surface of the glass building blocks, the design of thin film coatings as used in the next section for polarization control or wavelength separation is facilitated, as light reaches the coated surfaces with a narrow range of k-vectors.

Figure 3 shows transmission and cross-talk measurements between standard SMFs coupled by the glass interposer. (a) and (b) show transmission data in the O-band, with single mode fibers freely aligned on either side of the interposer in (a) and fibers constrained by a fixed FA position and a single alignment used for all measurements in (b). The ILs in (b) are slightly worse, as the facets of the fibers are constrained to be exactly in the planes of the interposer’s attachment surfaces, to which the FAs are flush. In addition, the relative position of the fibers on a given interposer side is constrained by them being encased inside an FA. ILs remain however better than 2 dB across the entire O- and C-

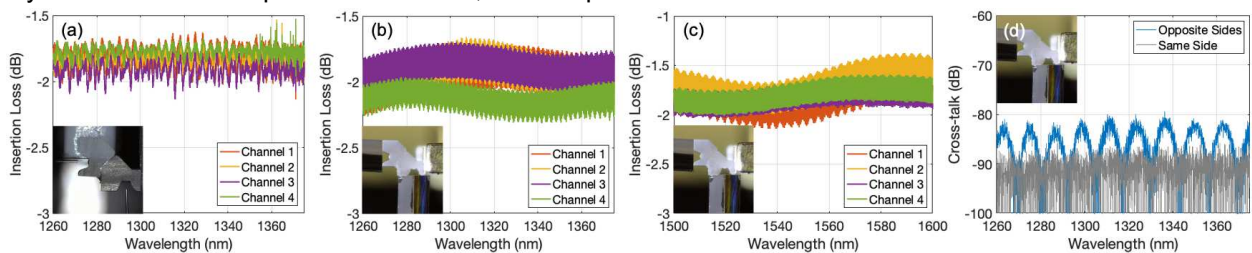


**Fig. 3:** Transmission and cross-talk measurements. (a) ILs for independent fibers, see inset. (b),(c) ILs in the O- and C-bands with rigid FAs (single alignment for all channels). (d) Cross-talk between fibers coupled to lens 1 and to lens 2, either on the same (black) or opposite (blue) side of the interposer. Here too, fibers are embedded in a rigid FA.

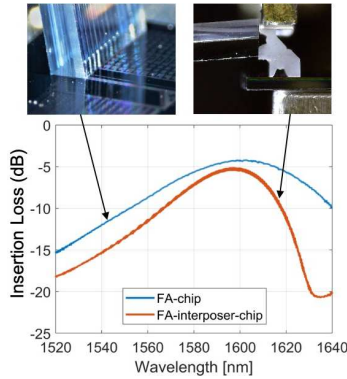


**Fig. 4:** ILs obtained from direct coupling of an FA to a PIC via a GC (left, blue curve) and from coupling of an FA to the PIC via a glass molded interposer (right, red curve). Low excess losses of 0.9 dB are measured, while enabling low footprint packaging and additional functionalities such as optical isolation.

bands, see panel (c). Panel (d) shows extremely low cross-talk data taken between fiber 1 on one side of the interposer and fiber 2 on either the same or the opposite side, below -80 dB.

The FAs used for these measurements were polished with a  $2^\circ$  angle and mechanically connected to the interposer with flush surfaces. The rays are thus fed into the interposer with a slight angle of  $\sim 3^\circ$ , after refraction at the FA glass-air interface, and are representative of a situation in which the bottom FA were to be replaced by a PIC using grating couplers (GCs) with a slight emission angle relative to the chip's surface normal. Since the incidence angle at the input of the interposer is mapped to its output, the coupling scheme is also compatible with straight emitters such as VCSELs provided a  $0^\circ$  polish FA is used. Due to the action of the lenses, rays remain on the cartesian grid inside the interposer in either case. Experiments were made coupling light from four fibers encased in an FA with a  $6^\circ$  polish to the four GC-ports of waveguide loops on a silicon photonics PIC fabricated in standard 220 nm thick device layer silicon-on-insulator (SOI). Excess losses recorded to be 0.9 dB per port for both loops (Fig. 4) are even better than for fiber-to-fiber coupling as the lens system partially compensates for mismatch to the GC beam.

### Polarization management and isolation

The previous section describes basic PIC-to-fiber coupling. Slightly more complex interposers can be built with the same basic elements to incorporate polarization management, isolation, or WDM. As an example, the interposer in Fig. 5 can either launch two polarizations into a single fiber with independent data streams at a polarization multiplexing Tx, or split light incoming from a fiber by polarization and route it to separate GCs at a Rx. In the Tx case, isolation can also be straightforwardly implemented by adding  $45^\circ$  Faraday rotators into the optical path between the PIC and the interposer, to protect an upstream laser from downstream reflections. In the Rx, light can be further processed on chip by recombining the two polarizations in a single photodetector<sup>[7]</sup>, including WDM signals<sup>[8,9]</sup>.

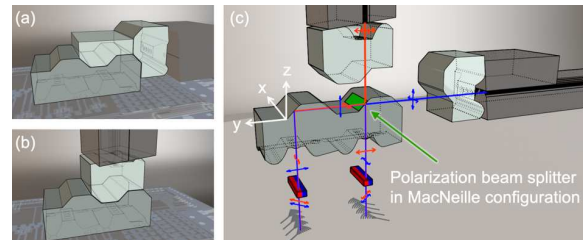


**Fig. 5:** Interposer with isolation and polarization control. (a),(b) Compact representation with FAs attached on either the side or the top of the interposer, for packaging module form factors and CPO, respectively. (c) Extrusion drawing with overlaid beam paths for both configurations (blue: FA attached on the side, red: FA attached on top with flipped Faraday rotators). Double sided arrows indicate the polarization of the light.

As seen in Figs. 5(a) and 5(b), the FA can either be brought in from the side, as in the previous section, or from the top. The stack-up of the elements and the beam paths are illustrated in the extrusion drawing shown in panel (c). The GCs on the PIC are oriented perpendicularly relative to each other in order to emit or receive the correct polarization. When a Faraday rotator is interposed in the optical path, the GCs are both rotated by an additional  $45^\circ$  in order to account for the induced polarization rotation, since, inside the interposer, the corresponding polarizations have to be along the x- and y-axes in order to implement a polarization splitter as a thin-film coating in the MacNeille configuration. In a polarization multiplexing transmitter, isolation is achieved by means of the Faraday rotators since returning light will have the opposite polarization than the one coupled by the emitting GC. To switch between side and top FA attachment, both GCs have to be rotated by an additional  $90^\circ$  to switch between p- and s-polarizations. Alternatively, the direction of rotation of the Faraday rotator can be switched, as represented in Fig. 5, in order to keep the same PIC. While the configuration with FA to the side requires a third glass building block, it is not significantly more difficult to assemble, as the latter does not need to be precisely aligned along the x-direction and the other alignments are simply guaranteed by mechanical contact. The position of lenses are shifted in some configurations to accommodate the angled emission of on-chip GCs, without adding complications to manufacturing.

These configurations can be extended to WDM by changing the types of coating. We are currently developing an additional interposer configuration that allows in-coupling a remote laser to a CPO transceiver with single mode fiber and modulating both polarizations with a single modulator without the need of an active polarization combiner<sup>[10,11]</sup>.

### Acknowledgements

Project EFFICIENTlight funded by the German Federal Ministry for Education and Research.

## References

- [1] E. R. H. Fuchs, R. E. Kirchain, and S. Liu, "The Future of Silicon Photonics: Not So Fast?," *J. Lightw. Technol.*, vol. 29, no. 15, pp. 2319-2326, 2011.
- [2] S. Fatholouloumi *et al.*, "1.6Tbps Silicon Photonics Integrated Circuit for Co-Packaged Optical-IO Switch Applications," in *Proc. Opt. Netw. Comm. Conf. & Exhibit. (OFC)*, Art. ID T3H.1, 2020.
- [3] F. A. I. Chaqmaqchee and J. A. Lott, "Impact of oxide aperture diameter on optical output power, spectral emission, and bandwidth for 980 nm VCSELs," *OSA Cont.*, vol. 3, no. 9, pp. 2602-2613, 2020.
- [4] S. Romero-García *et al.*, "Alignment Tolerant Couplers for Silicon Photonics," *J. Sel. Top. Quant. Electron.*, vol. 21, no. 6, Art. ID 8200214, 2015.
- [5] I. Ghannam *et al.*, "Silicon Photonics External Cavity Laser with Misalignment Tolerant Multi-mode RSOA to PIC Interface," in *Proc. Conf. Las. & Electr.-Opt. (CLEO)*, Art. ID AT31.3, 2019.
- [6] M. Hüntgen, F. Klocke, O. Dambon, "Precision glass molding: an integrative approach for the production of high precision micro-optics," in *Proc. SPIE*, vol. 7591, Art. ID 75910X, 2010.
- [7] D. Kucharski *et al.*, "10-Gb/s 15-mW Optical Receiver with Integrated Germanium Photodetector and Hybrid Inductor Peaking in 0.13  $\mu\text{m}$  SOI CMOS Technology," in *Proc. Int. Sol.-State Circ. Conf. (ISSCC)*, pp. 360-362, 2010.
- [8] A. H. K. Park *et al.*, "Ring resonator based polarization diversity WDM receiver," *Opt. Expr.*, vol. 27, no. 5, pp. 6147-6157, 2019.
- [9] J. Nojic, D. Schoofs, S. Sharif Azadeh, F. Merget, and J. Witzens, "Polarization-diverse silicon photonics WDM receiver with a reduced number of OADMs and balanced group delays," in *Proc. Opt. Fib. Comm. Conf. (OFC)*, Art. ID M4H.2, 2020.
- [10] A. Mekis, A. Narasimha, J. Witzens, "Method and System for Interated Power Combiners," US Patent 9417466B2, Jun. 2011.
- [11] H. Zhou *et al.*, "All-in-one silicon photonics polarization processor," *Nanophotonics*, vol. 8, no. 12, pp. 2257-2267, 2019.